

## The Distance to the M31 Globular Cluster System

Stephen Holland

Institut for Fysik og Astronomi

Aarhus Universitet

Ny Munkegade, Bygning 520

DK-8000 Århus C

Denmark

### ABSTRACT

The distance to the centroid of the M31 globular cluster system is determined by fitting theoretical isochrones to the observed red-giant branches of fourteen globular clusters in M31. The mean true distance modulus of the M31 globular clusters is found to be  $\mu_0 = 24.47 \pm 0.07$  mag. This is consistent with distance moduli for M31 that have been obtained using other distance indicators.

*Subject headings:* galaxies: distances and redshifts — galaxies: individual (M31) — galaxies: star clusters

### 1. Introduction

Over the last ten years the distance to the Andromeda Galaxy (= M31 = NGC 224) has been measured using a variety of distance indicators. Pritchett & van den Bergh (1987) used RR Lyrae variables to derive a true distance modulus of  $24.34 \pm 0.15$ . The observed brightnesses of red giants in the halo of M31 suggest that  $\mu_0 = 24.23 \pm 0.15$  (Pritchett & van den Bergh 1988). Novae light curves give a distance modulus of  $24.27 \pm 0.20$  (Capaccioli et al. 1989) while Cepheid variables suggest that  $\mu_0 = 24.43 \pm 0.06$  (Freedman & Madore 1990). Brewer et al. (1995) found  $\mu_0 = 24.36 \pm 0.03$  using carbon stars in the disk of M31 yet Ostriker & Gnedin (1997) found  $\mu_0 = 24.03 \pm 0.23$  from the peak of M31's globular cluster (GC) luminosity function. A weighted mean of these six values yields  $\langle \mu_0 \rangle = 24.36 \pm 0.03$  mag where the uncertainty is the standard error in the mean. This corresponds to a distance of  $\sim 745$  kpc.

Recently Feast & Catchpole (1997) used *Hipparcos* data to calibrate the Cepheid period–luminosity (PL) relation and found a distance modulus of  $\mu_0 = 24.77 \pm 0.11$  for M31. This corresponds to a distance of  $\sim 900$  kpc, an increase of  $\sim 20\%$  over the previously accepted value. However, Madore & Freedman (1997) analysed the *Hipparcos* data and found that the

pre-*Hipparcos* zero point for the Cepheid PL relation is good to within  $\pm 0.14$  mag ( $\sim 7\%$ ). They also note that uncertainties due to reddening, metallicity effects on the PL relation, and statistical uncertainties in the data make up a significant component of the total uncertainty in the PL zero point.

This study determines an estimate of the distance to M31 by finding the distance to the centroid of the M31 GC system. The shape of the red-giant branch (RGB) in a GC is strongly sensitive to the metallicity of the GC (see Da Costa & Armandroff 1990 for a discussion of this effect in Galactic GCs). If the metallicity of the GC is determined in a manner that is *independent of the distance to the GC*, and the amount of reddening along the line-of-sight to the GC is known, then a reference isochrone of the correct metallicity can be shifted in distance until the best fit to the GC’s RGB is obtained.

## 2. The Data

### 2.1. The Red-Giant Branches

The RGB data used in this study were taken from three sources. RGB fiducial sequences for G1, G58, G105, G108, G280, G219, and G351 were taken from Table 2 of Fusi Pecci et al. (1996, hereafter referred to as FP96). These fiducial sequences represent the observed mean points of the RGBs *before* reddening and extinction corrections were applied. The fiducial sequences for G302 and G312 were obtained by drawing mean lines through the RGBs of each GC using the data from Holland et al. (1997, hereafter referred to as HFR). The data for these two GCs were recalibrated using the procedure described in HFR but with no reddening or extinction corrections applied. The fiducial sequences for G11, G319, G323, G327, and G352 were obtained by drawing mean lines through the RGBs of each GC using the data in Couture et al. (1995, hereafter referred to as CR95). The fiducial sequences for these five GCs were dereddened, and extinction corrections removed, by inverting the reddening and extinction corrections described in CR95.

FP96 used  $B$ -,  $V$ -, and  $I$ -band photometry from the Wide-Field Planetary-Camera 2 (WFPC2) aboard the *Hubble Space Telescope* (*HST*) to construct their color–magnitude diagrams (CMDs). HFR used WFPC2  $V$ - and  $I$ - band photometry while CR95 used  $V$ - and  $I$ -band photometry from the High Resolution Camera at the Canada–France–Hawaii telescope (CFHT). The data for G280 and G351 are from  $B$ - and  $V$ -band photometry with the Faint Object Camera aboard the *HST*. The limiting magnitudes (the  $V$ -band magnitude where the published uncertainties in the photometry for the individual stars is  $\sigma_V \sim 0.1$ ) for the *HST* CMDs are  $V_{\text{lim}} \sim 26$ . For the CFHT data  $V_{\text{lim}} \sim 23$ . The fiducial sequence for Bo468 (from FP90) was not used since there is no published estimate of its iron abundance that was obtained using a method that does not require prior knowledge of the distance to the GC.

Uncertainties were assigned to the fiducial points based on the width of the observed RGB

at each fiducial point. The width of the RGB was measured and assumed to be 1.5 times the Full-Width at Half-Maximum (i.e. the bin has a half-width of  $\sim 3.5\sigma$ ) of the scatter around the mean point. This assumes that the scatter is due to Gaussian uncertainties in the photometry. It ignores complications due to confusion between RGB and asymptotic giant branch stars, binary stars, and contamination from stars in the halo of M31. This means that the uncertainties can not be used as a measure of the quality of individual fiducials. However, they can be used to provide an estimate of the relative weight to give each fiducial point *in a single GC's RGB*.

## 2.2. The Iron Abundances

The iron abundances used in this study were taken from the Huchra et al. (1991) catalogue of iron abundances and radial velocities for 150 GCs in the M31 system. These iron abundances were determined using six absorption lines indices measured from integrated spectra of each GC and a calibration that was tied to the metallicity scale of Zinn & West (1984). The method is fully described in Brodie & Huchra (1990). These iron abundances are completely independent of the distance to M31, the amount of interstellar reddening, and the stellar photometry used to generate the RGB fiducial sequences for the GCs. Other methods of estimating the iron abundances of M31 GCs, such as integrated colors (e.g. Bònoli et al. 1987) and CMD-based methods (e.g. HRF), require a knowledge of either the amount of reddening along the line-of-sight to the GC, or the distance to M31, or both. Therefore only spectroscopic estimates of the iron abundance are used in this study. FP96 found that Huchra et al.'s (1991) spectroscopic iron abundances were consistent with the iron abundances obtained from integrated colors for all of the GCs in their sample except G280, assuming a distance modulus of  $\mu_0 = 24.43$  for M31.

## 2.3. The Isochrones

In order to determine the distance to each GC the fiducial RGB sequences for each GC were compared to theoretical isochrones. This procedure is described in greater detail in Sec. 3. The oxygen enhanced isochrones of VandenBerg (1997), with an age of  $t_0 = 14$  Gyr, were used. This assumes that the M31 GC system has the same age as the Galactic GC system. The choice of age is not critical since location of the RGB shifts by only  $d(V-I)/dt_0 \sim 0.008$  mag/Gyr at  $M_V \sim -1$ , which is small compared to the uncertainties in the reddening and in the spectroscopic iron abundance for each GC. An alpha-element enhancement of  $[\alpha/\text{Fe}] = +0.3$  was adopted since this amount of alpha-element enhancement is seen in Galactic GCs with a wide range of iron abundances (see Carney 1996). The color transformations used to transform the isochrones from the  $(M_{\text{bol}}, T_{\text{eff}})$  plane to the  $(M_V, V-I)$  plane give good fits up to  $[\text{Fe}/\text{H}] \sim -0.8$  but may be less reliable for higher iron abundances (VandenBerg, private communication).

For each GC an isochrone of the appropriate iron abundance was obtained by interpolating

across a grid of reference isochrones. This is not a formally correct method of obtaining isochrones with specific iron abundances. However, none of the interpolations were more than 0.08 dex away from a reference isochrone so the error introduced by the interpolation will be small compared to the uncertainties in the spectroscopic iron abundance measurements ( $\langle\sigma_{[\text{Fe}/\text{H}]}\rangle = 0.23$  dex).

## 2.4. The Reddenings

The reddening in the direction of each GC was determined using the  $E_{B-V}$  reddening maps of Burstein & Heiles (1982). The uncertainties in the  $E_{B-V}$  values are approximately 0.01 mag due to uncertainties in the reddening maps and the interpolation process. The  $E_{B-V}$  values were converted to  $E_{V-I}$  values using  $E_{V-I} = 1.36E_{B-V}$  (Taylor 1986, Fahlman et al. 1989). G58 and G108 are located near NGC 205, which may lead to less accurate reddening estimates for these two GCs. An interstellar extinction of  $A_V = (3.09 \pm 0.03)E_{B-V}$  (Rieke & Lebofsky 1985), where the quoted uncertainty is the  $2\sigma$  uncertainty, was adopted. The comparison isochrone for each GC was reddened by the appropriate amount for each GC and the appropriate extinction corrections were applied.

A summary of the properties of each GC is given in Table 1. The GC names are from Sargent et al. (1977) except for Bo468, which is from Battistini et al. (1987). The integrated  $V$ -band magnitudes ( $V$ ) and projected distances from the centre of M31 ( $R$ ) are from Huchra et al. (1991). The exception is the coordinates and projected distance for Bo468, which are from Battistini et al. (1987). The reference (column 8) gives the source of the CMD for that GC.

## 3. The Results

The distance modulus for each GC was found by computing the weighted mean difference between the observed  $V$ -band magnitude of the  $i^{\text{th}}$  fiducial point,  $V_i$ , and the absolute  $V$ -band magnitude of the comparison isochrone (after correcting for reddening and extinction) at the same  $V-I$  colour as the fiducial point,  $M_V((V-I)_i)$ . The procedure for G280 and G351, for which  $B$ - and  $V$ -band photometry is available, is the same except that the  $B-V$  colour index was used instead of the  $V-I$  colour index. The formula for the distance modulus,  $\mu_0$ , and its formal uncertainty,  $\sigma_{\mu_0}$  is:

$$\mu_0 = \left( \sum_{i=1}^N \frac{V_i}{w_i} - \sum_{i=1}^N \frac{M_V((V-I)_i)}{w_i} \right) / \sum_{i=1}^N \frac{1}{w_i} \pm \sqrt{\sum_{i=1}^N \frac{1}{w_i}}, \quad (1)$$

where  $w_i$  is the weight assigned to the  $i^{\text{th}}$  fiducial point and  $N$  is the number of fiducial points. The weights were set to  $w_i = \sigma_{V-I,i}^2 + \sigma_{V,i}^2$  where  $\sigma_{V-I,i}$  and  $\sigma_{V,i}$  are the uncertainties in the location of the  $i^{\text{th}}$  fiducial point (see Sec. 2.1). The formal uncertainties in the individual distance moduli

do not include uncertainties in the reddening or uncertainties in the iron abundance estimates since these uncertainties would be constant for a given GC.

The uncertainty in  $\mu_0$  for each GC due to the uncertainty in the adopted reddening was estimated by recomputing  $\mu_0$  using  $E_{B-V} + \sigma_{E_{B-V}}$  and  $E_{B-V} - \sigma_{E_{B-V}}$  then taking half of the difference between the resulting  $\mu_0$ s. The uncertainty in  $\mu_0$  for each GC due to the uncertainty in the spectroscopic iron abundance was estimated in the same manner using  $[\text{Fe}/\text{H}] + \sigma_{[\text{Fe}/\text{H}]}$  and  $[\text{Fe}/\text{H}] - \sigma_{[\text{Fe}/\text{H}]}$ . The results are presented in Table 2 along with the quadratic sum of all three sources of error. Table 2 also lists the best-fit values of the distance modulus for each GC along with the uncertainties in each fit, the root-mean-square (RMS) scatter in the fit, and the number of fiducial points used to make the fit. Figures 1 and 2 shows the best-fits between the fiducial sequences and the comparison isochrones.

The uncertainties in the individual distance moduli are dominated by the uncertainties in either the reddening estimate or iron abundance determination. An examination of the reddening maps of Burstein & Heiles (1982) shows that the spatial scale of variations in reddening in the direction of M31 is larger than the typical projected distances between the GCs. This means that uncertainties in the reddenings will not be completely independent from one GC to another. Uncertainties in the spectroscopic iron abundances due to errors subtracting the continuum will result in systematic errors in  $[\text{Fe}/\text{H}]$ . Recent results have suggested that the Huchra et al. (1991) iron abundances may be systematically underestimated for the metal-rich GCs (Seitzer, private communication; de Freitas Pacheco 1997; Ponder et al. 1994). Increasing the iron abundance in GC stars will result in the upper RGB turning over to become flatter and redder than the upper RGB of metal-poor GCs are. Therefore, underestimating the iron abundance of a GC will result in fitting a comparison isochrone that is too bright, which will lead to the fitted distance of that GC being larger than the true distance. Therefore, a systematic error in the measured iron abundance of a GC will lead to a systematic error in the derived distance modulus of that GC that increases as the iron abundance increases.

Since the uncertainties have a systematic component, and the size of this systematic component is unknown, they could not be used to weight the individual distance moduli when computing the mean distance modulus. Therefore, unweighted distance moduli were used to compute the distance to the centroid of the M31 GC system. The unweighted mean distance modulus for all the GCs in Table 2 is  $\langle \mu_0 \rangle = 24.47 \pm 0.07$  mag. All quoted uncertainties are standard errors in the means unless otherwise stated.

In order to test for effects arising from a possible systematic under-estimate of the iron abundances of the iron-rich GCs the sample of GCs was divided into two groups containing seven GCs each. The iron-poor group consisted of those GCs with  $[\text{Fe}/\text{H}] < -1.2$  dex while the iron-rich group was made up of those GCs with  $[\text{Fe}/\text{H}] > -1.2$  dex. The unweighted mean distance moduli computed for each group were  $\langle \mu_0 \rangle = 24.41 \pm 0.14$ , for  $[\text{Fe}/\text{H}] < -1.2$ , and  $\langle \mu_0 \rangle = 24.53 \pm 0.06$ , for  $[\text{Fe}/\text{H}] > -1.2$ . The Student's  $t$ -test gives a probability of obtaining these two means by chance

from a single distribution of 42.87%. Therefore, there is no evidence that the derived distances of the iron-rich GCs are greater than those of the iron-poor GCs.

The quality of the individual CMDs that were used to obtain the RGB fiducial sequences varies greatly. In addition, the photometry was obtained using three different instruments and calibrated using different procedures (see CR95, FP96, and HFR for details). In order to eliminate any systematic effects arising from the combination of several different data sets the unweighted mean of the distance moduli of the GCs observed with the WFPC2 and calibrated by FP96 was computed. This is the largest self-consistent subset of GCs ( $N = 5$ ) available. The unweighted mean is  $\langle\mu_0\rangle = 24.37 \pm 0.06$ , which is within  $1.5\sigma$  of the mean of the entire sample of GCs.

#### 4. Conclusions

The distances to fourteen GCs in the M31 system have been estimated by comparing the observed RGB of each GC to a theoretical isochrone with the same iron abundance. The unweighted mean distance modulus of the GCs is  $\langle\mu_0\rangle = 24.47 \pm 0.07$  mag. If only the “best” data set (the largest data set that used the same instrument and calibrations) is used a distance modulus of  $\langle\mu_0\rangle = 24.37 \pm 0.06$  mag is obtained. These estimates of the distance to M31 are consistent with distances obtained using other techniques and do not support the need for a revision of the distance to M31.

This method of determining the distance to M31 depends on accurate iron abundance estimates for the individual GCs and needs a sample of M31 GCs with high-precision photometry of their RGB stars. In order to improve the accuracy of this distance estimator deep ( $V_{\text{lim}} \gtrsim 26$ ) photometry will be needed for a much larger sample of M31 GCs. In addition, further work needs to be done to reduce the uncertainties in the spectroscopic iron abundance measurements of M31 GCs.

This research is based, in part, on observations made with the NASA/ESA *Hubble Space Telescope* obtained at the Space Telescope Science Institute. STScI is operated by the Association of Universities for Research in Astronomy Inc. under NASA contract NAS5–26555. This research is also based, in part, on observations made with the Canada–France–Hawaii Telescope operated by the National Research Council of Canada, the Centre National de la Recherche Scientifique de France and the University of Hawaii. The author would like to thank Don Vandenberg for kindly providing copies of the isochrones used in this study.

## REFERENCES

- Battistini, P., Bònoli, F., Braccisi, A., Federici, L., Fusi Pecci, F., Marano, B., & Borngen, F. 1987, *A&AS*, 67, 447
- Bònoli, F., Delpino, F. E., Federici, L., & Fusi Pecci, F., 1987, *A&A*, 185, 25
- Brewer, J. P., Richer, H. B., & Crabtree, D. R. 1995, *AJ*, 109, 2480
- Brodie, J. P., & Huchra, J. P. 1990, *ApJ*, 362, 503
- Burstein, D., & Heiles, C. 1982, *AJ*, 87, 1165
- Capaccioli, M., Della Valla, M., Rosino, L., & D’Onofrio, M. 1989, *AJ*, 97, 1622
- Carney, B. W., 1996, *PASP*, 108, 900
- Couture, J., Racine, R., Harris, W. E., & Holland, S. 1995, *AJ*, 109, 205 (CR95)
- Da Costa, G. S., & Armandroff, T. E. 1990, *AJ*, 100, 162
- de Freitas Pacheco, J. A. 1997, *A&A*, 319, 394
- Fahlman, G. G., Richer, H. B., Searle, L., & Thompsom, I. B. 1989, *ApJ*, 343, L51
- Feast, M. W., & Catchpole, R. M., 1997, *MNRAS*, 286, L1
- Freedman, W. L., & Madore, B. F., 1990, *ApJ*, 365, 186
- Fusi Pecci, F., Buonanno, R., Cacciari, C., Corsi, C. E., Djorgovski, S. G., Federici, L., Ferraro, F. R., Parmeggiani, G., & Rich, R., M. 1996, *AJ*, 112, 1461 (FP96)
- Holland, S., Fahlman, G. G., & Richer, R. B. 1997, *AJ*, 114, 1488 (HFR)
- Huchra, J. P., Brodie, J. P., & Kent, S. M. 1991, *ApJ*, 370, 495
- Madore, B. F., & Freedman, W. L., 1997, *ApJ*, 492, 517
- Ostriker, J. P., & Gnedin, O. Y. 1997, *ApJ*, 487, 667
- Ponder, J., Burstein, D., Wu, C.-C., O’Connell, R. W., Rose, J. A., Frogel, J. A., & Rieke, M. 1994, *BAAS*, 185, #104.15
- Pritchett, C. J., & van den Bergh, S. 1987, *ApJ*, 316, 517
- Pritchett, C. J., & van den Bergh, S. 1988, *ApJ*, 331, 135
- Rieke, G. H., & Lebofsky, M. J. 1985, *ApJ*, 288, 618
- Sargent, W. L. W., Kowal, C. T., Hartwick, F. D. A., & van den Bergh, S. 1977, *AJ*, 82, 947
- Taylor, B. J. 1986, *ApJS*, 60, 577
- VandenBerg, D. A. 1997, in preparation
- Zinn, R., & West, M. 1984, *ApJS*, 55, 45

Table 1. Properties of the globular clusters.

Cluster	$\alpha_{J2000}$	$\delta_{J2000}$	$V$	$R$	[Fe/H]	$E_{B-V}$	Ref.
G1	00 <sup>h</sup> 32 <sup>m</sup> 46 <sup>s</sup> .8	+39°34'42''	13.70	152'3	$-1.08 \pm 0.09$	0.06	2
G11	00 <sup>h</sup> 36 <sup>m</sup> 20 <sup>s</sup> .5	+40°53'38''	16.39	75'7	$-1.89 \pm 0.17$	0.06	1
G58	00 <sup>h</sup> 40 <sup>m</sup> 26 <sup>s</sup> .8	+41°27'28''	15.80	28'2	$-0.57 \pm 0.15$	0.06	2
G105	00 <sup>h</sup> 41 <sup>m</sup> 42 <sup>s</sup> .2	+40°12'23''	16.35	64'8	$-1.49 \pm 0.17$	0.06	2
G108	00 <sup>h</sup> 41 <sup>m</sup> 43 <sup>s</sup> .3	+41°33'32''	15.80	20'8	$-0.94 \pm 0.27$	0.09	2
Bo468	00 <sup>h</sup> 43 <sup>m</sup> 12 <sup>s</sup> .5	+39°47'57''	18.12	87'0	...	0.06	2
G219	00 <sup>h</sup> 43 <sup>m</sup> 18 <sup>s</sup> .0	+39°49'14''	15.10	87'2	$-1.83 \pm 0.22$	0.06	2
G280	00 <sup>h</sup> 44 <sup>m</sup> 29 <sup>s</sup> .9	+41°21'37''	14.30	20'5	$-0.70 \pm 0.12$	0.06	2
G302	00 <sup>h</sup> 45 <sup>m</sup> 25 <sup>s</sup> .2	+41°05'30''	14.90	32'1	$-1.76 \pm 0.18$	0.08	3
G312	00 <sup>h</sup> 45 <sup>m</sup> 58 <sup>s</sup> .8	+40°42'32''	16.05	48'9	$-0.70 \pm 0.35$	0.08	3
G319	00 <sup>h</sup> 46 <sup>m</sup> 22 <sup>s</sup> .1	+40°17'00''	15.75	72'1	$-0.66 \pm 0.22$	0.07	1
G323	00 <sup>h</sup> 46 <sup>m</sup> 33 <sup>s</sup> .6	+40°44'14''	17.09	53'8	$-1.96 \pm 0.29$	0.07	1
G327	00 <sup>h</sup> 46 <sup>m</sup> 49 <sup>s</sup> .4	+42°44'49''	16.00	99'7	$-1.76 \pm 0.11$	0.12	1
G351	00 <sup>h</sup> 49 <sup>m</sup> 33 <sup>s</sup> .1	+41°35'32''	15.18	79'0	$-1.80 \pm 0.31$	0.09	2
G352	00 <sup>h</sup> 50 <sup>m</sup> 10 <sup>s</sup> .0	+41°41'01''	16.01	87'1	$-0.85 \pm 0.33$	0.09	1

References. — (1) Couture et al. (1995); (2) Fusi Pecci et al. (1996); (3) Holland et al. (1997).

Table 2. The best-fitting distance moduli for each GC.

Cluster	$\mu_0$	$\sigma_{\mu_0}(\text{fit})^{\text{a}}$	$\sigma_{\mu_0}(E_{B-V})^{\text{b}}$	$\sigma_{\mu_0}([\text{Fe}/\text{H}])^{\text{c}}$	$\sigma_{\mu_0}(\text{total})^{\text{d}}$	RMS	$N$
G1	24.53	0.03	0.05	0.07	0.09	0.448	8
G11	24.80	0.03	0.11	0.07	0.13	0.078	7
G58	24.39	0.02	0.06	0.06	0.09	0.204	10
G105	24.35	0.01	0.09	0.31	0.32	0.089	9
G108	24.40	0.02	0.04	0.57	0.57	0.236	10
G219	24.18	0.01	0.11	0.02	0.11	0.071	9
G280	24.86	0.04	0.05	0.09	0.11	0.300	8
G302	24.23	0.01	0.10	0.03	0.10	0.386	11
G312	24.42	0.01	0.07	0.21	0.22	0.140	11
G319	24.49	0.05	0.08	0.21	0.23	0.429	6
G323	24.31	0.03	0.11	0.04	0.12	0.037	8
G327	23.98	0.04	0.11	0.13	0.17	0.505	5
G351	25.01	0.04	0.08	0.15	0.17	0.293	7
G352	24.64	0.03	0.04	0.18	0.19	0.070	6

<sup>a</sup>The formal uncertainty in the fit, from Equation 1.

<sup>b</sup>The uncertainty due to uncertainties in the reddening.

<sup>c</sup>The uncertainty due to uncertainties in the iron abundance.

<sup>d</sup>The total uncertainty in  $\mu_0$ .

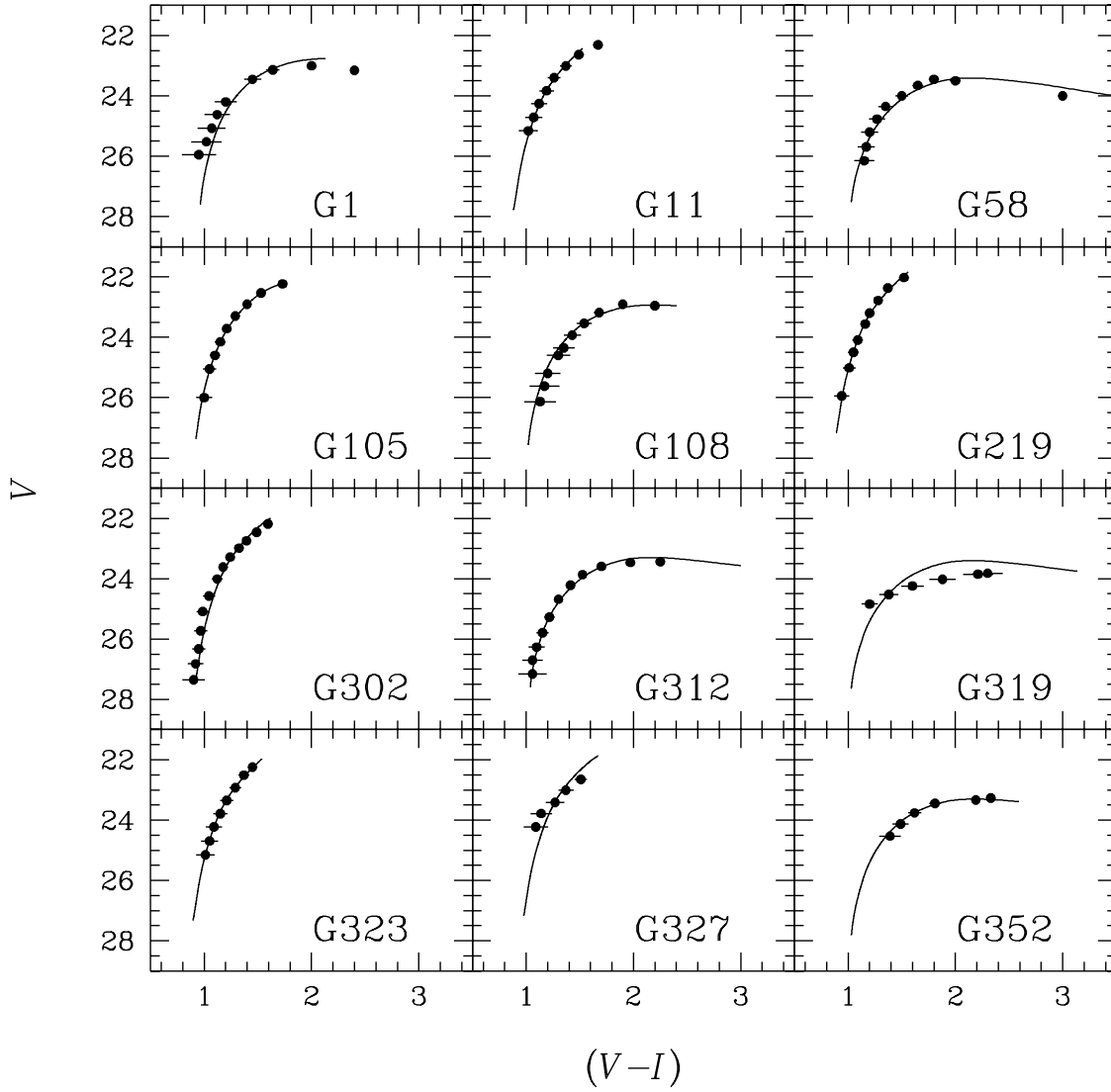


Fig. 1.— The RGB fiducial sequences for each GC with  $V$ - and  $I$ -band data available. The best-fitting isochrones has been overlaid on each RGB. The isochrones have been reddened and adjusted for interstellar extinction as described in Sec. 2.4.

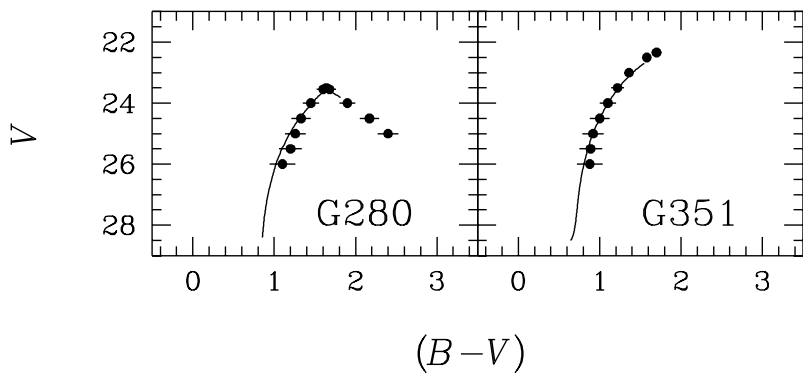


Fig. 2.— The RGB fiducial sequences for each GC with  $B$ - and  $V$ -band data available. The best-fitting isochrones has been overlaid on each RGB. The isochrones have been reddened and adjusted for interstellar extinction as described in Sec. 2.4.